Indian Journal of Geo Marine Sciences
Vol. 48 (05), May 2019, pp. 730-738

A new algorithm for high-precision submarine topography imaging

Jingsheng Zhai, Bo Zou, Jian Xu*, & Sunpei Gao
School of Marine Science and Technology, Tianjin University, Tianjin, China
*[E-mail: jian.xu@tju.edu.cn]

Received 14 November 2017; revised 9 May 2018

In this paper, a new algorithm for high-precision submarine topography imaging is proposed. The innovative idea comes from the most effective and widely used instruments: Multibeam echo sounder (MBES) and side scan sonar (SSS). The MBES can acquire bathymetric information with high precision, but its along-track resolution is related to the result of the beam angle multiplied by the slant range. The SSS combined with synthetic aperture sonar technology can achieve a high-precision along-track imaging resolution, but it cannot acquire bathymetric information directly below it. The proposed algorithm uses the beam footprints of the MBES in the along-track direction to perform the aperture synthesis and uses the time-domain and beam-domain imaging algorithms to acquire high-precision along-track imaging resolution and bathymetric information, to improve the along-track resolution and obtain the bathymetric information with high precision at the same time. Finally, an experiment is performed to evaluate the effectiveness of our method. Experimental results demonstrate that two targets, 13 cm in size, can be clearly observed from the obtained imaging. Moreover, their bathymetric information can be calculated by using the beamforming angle information.

[**Keywords:** Sonar; Resolution; Multibeam; Imaging]

Introduction

Submarine topography imaging takes a very important role within marine scientific research, which, in turn, occupies a very important position within the study of geosciences. At present, the underwater acoustic signal is the only information carrier which can propagate a long distance in the sea. Therefore, the submarine topography imaging technology based on underwater acoustic signals is the most important method for marine scientific research.

Recently, underwater acoustic submarine topography imaging technology has been divided into two types: Long distances where global research is done by using marine mapping sonar[1,4]multibean echo sounder (MBES) and side scan sonar(SSS), as shown in Figure 1 and short distances where global research is done by using the high-frequency imaging sonar (lens sonar) [5], as shown in Figure 2.

With the development of marine scientific research, the needs of small-target and weak scattering-target submarine topography imaging have been significantly promoted. Scientists earnestly need the simultaneous output of both high-precision imaging and bathymetric information in the submarine region. The SSS combined with SAS

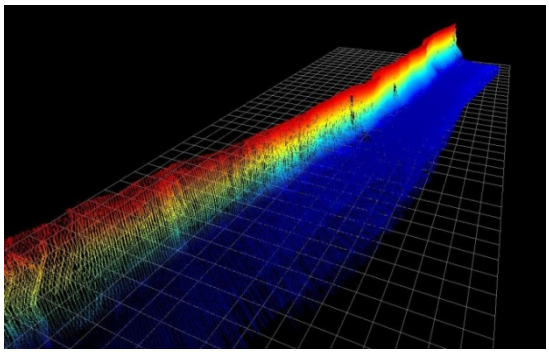

(a) The imaging results of the MBES

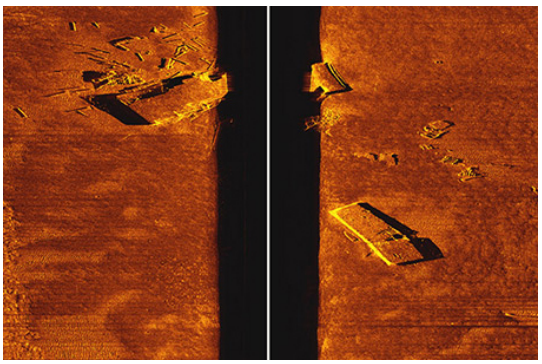

(b) The imaging results of the SSS

Fig. 1 — The imaging results of marine mapping sonar technologies.

technology can achieve the along-track high-precision imaging resolution required, but it cannot acquire the bathymetric information directly below the carrier[6,8]. The MBES can acquire the bathymetric information with high precision, but its along-track resolution is related to the result of the beam angle multiplied by the slant range[9,11]. Given the advantages of marine mapping sonar and high-frequency imaging sonar, the fusion of these two technologies has become a hot research topic.

To meet this need, a new algorithm for high-precision submarine topography imaging is proposed. This algorithm uses the multibeam echo sounder along-track beam footprints to perform the aperture synthesis and the time-domain and beam-domain imaging algorithm to achieve the high-precisionalong-track imaging resolution and the high-precision bathymetric information.

The contributions of this paper can be summarized as:

- The geometric models are provided to describe the along-track and bathymetric resolution of MBES, SSS, and SAS.
- The high-precision submarine topography imaginggeometric model and mechanism model of this paper are proposed.
- Based on the water-tank experiment results, the effectiveness and accuracy of the high-precision submarine topography imaging algorithm is verified.

Submarine Topography Imaging Algorithm

MBES imaging algorithm

The key of the MBES imaging algorithm is the beamforming algorithm[12,13]. The MBES imaging algorithm uses the beamforming algorithm to form several beams in the across-track directions. The bathymetric information of the seafloor is estimated by the arrival time and angle of the echo. As shown in Figure 3, the across-track azimuth of the MBES is the across-track beam width β_n. Based on the assumption that the time of echo arrival (TOA) is$t$, the bathymetric informationH_0 can be expressed as:

$$H_0 = \frac{1}{2} ct \cos \beta_n \quad \ldots (1)$$

The MBES imaging resolution can be divided into two parts: Across-track resolution and along-track resolution. From[14,15] we can see that the MBES imaging algorithm can obtain a satisfactory range

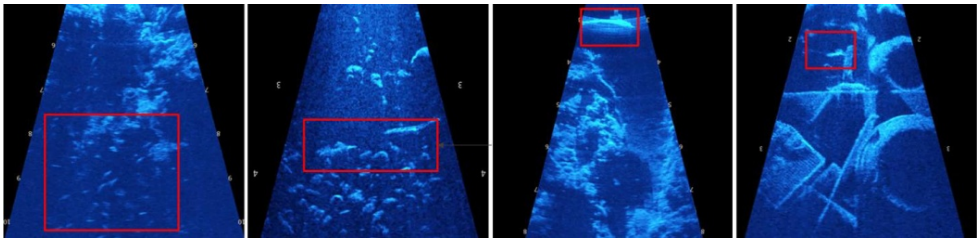

Fig. 2 — The imaging results of high-frequency image sonar technology.

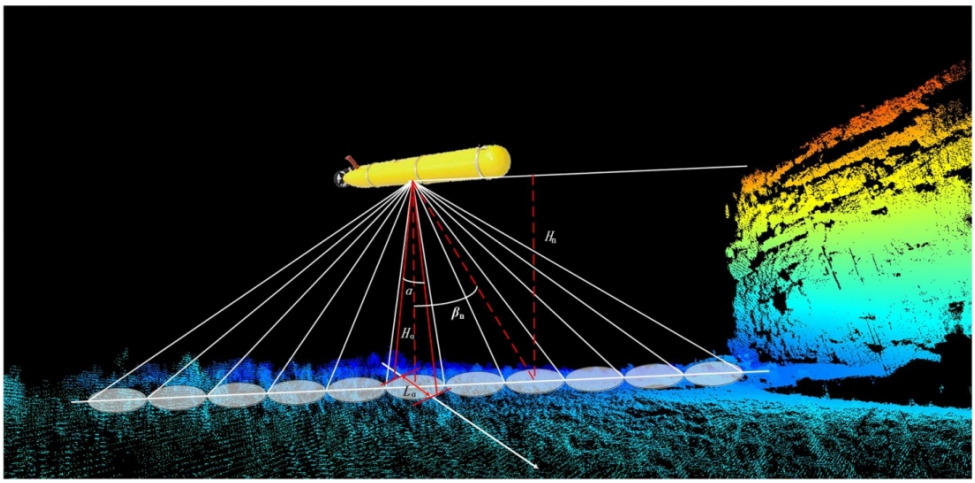

Fig. 3 —Geometric model of the MBES imaging algorithm

resolution and across-track resolution based on the multiple sub-array detection method, and can be expressed as:

$$\delta_{x\_MBES} = H_0[\tan(\beta_n + \beta_0/2) - \tan(\beta_n + 3\beta_0/2)] \quad \ldots (2)$$

For the MBES, its along-track resolution is related to the beam angle and the slant range. Assuming[16] the conventional transmitting array's along-track real aperture size is D and the wavelength of the transmit signal is λ, the transmit beam's angle of $-3dB$half-power point can be written as:

$$\alpha = \frac{\lambda}{D} \quad \ldots (3)$$

Its along-track resolution can be written as:

$$\delta_{y\_MBES} = \frac{\alpha H_0}{\cos\beta_n} = \frac{\lambda H_0}{D\cos\beta_n} \quad \ldots (4)$$

From formula (4), the following observations can be made:

- The real aperture size D is inversely proportional to the along-track resolution δ_{y_MBES}. If the real aperture size is larger, the along-track resolution is better. However, because the real aperture physical size cannot be increased without limit, it is very difficult to apply this method in practice to obtain a high-precision along-track resolution.
- The along-track resolution δ_{y_MBES} is proportional to the slant range $\frac{H_0}{\cos\beta_n}$ of the target. If the slant range of the target increases, the along-track resolution decreases.
- The transmitting signal's wavelength λ is proportional to the along-track resolution δ_{y_MBES}. If the transmitted signal wavelength is shortened, the along-track resolution increases. However, when the transmit signal's frequency is greatly increased, the transmission distance is affected due to the sound absorption of water[17]. Thus, it is very difficult to increase the along-track resolution.

SSS imaging algorithm

The key of the SSS imaging algorithm is the matched filtering algorithm (MFP), which is used to enhance the filtering effect and anti-jamming ability, and is advantageous for underwater target identification. As shown in Figure 4, the along-track resolution of traditional SSS is similar to that of MBES, which can be described as:

$$\delta_{y\_SSS} = R\alpha \quad \ldots (5)$$

where R is the slant range. The across-track resolution of traditional SSS is related to the form of transmitting signal and the grazing angle of the sound path. According to the matched filtering algorithm, when the transmitting signal is an LFM signal, the across-track resolution can be expressed as:

$$\delta_{x\_SSS} = \frac{c}{2B}\frac{1}{\cos\gamma} \quad \ldots (6)$$

where c stands for the sound velocity, B is the bandwidth of the transmitting signal and γ is the grazing angle.

Recently, scientists have applied the synthetic aperture technology to improve the performance of

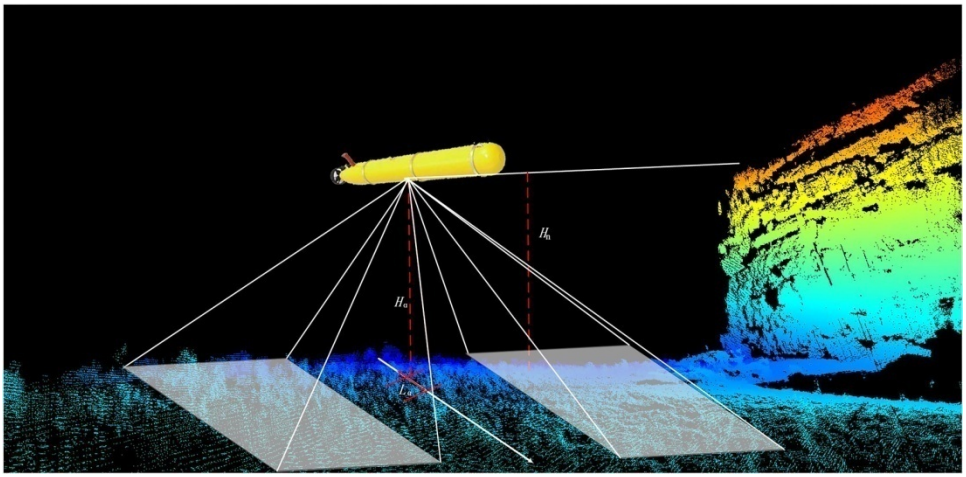

Fig. 4 — Geometric model of the SSS imaging algorithm.

SSS, which is called Synthetic aperture sonar (SAS). The SAS can acquire a virtual large aperture to achieve a high-precision along-track resolution through coherently combining signals received by a real aperture at different locations.The across-track and along-track resolution can be expressed as[18]:

$$\delta_{x\_SAS} = \frac{c}{2B} \quad \ldots (7)$$

$$\delta_{y\_SAS} = \frac{D}{2} \quad \ldots (8)$$

The SAScan acquire the bathymetric information by using the phase differences received from the additional receiving array[19,22]. The accuracy of these bathymetry algorithms, however, cannot reach the magnitude of the MBES. The bathymetric information directly below the SSS cannot be obtained and therefore has a gap problem.

Multibeam synthetic aperture high-precision submarine topography imaging algorithm

To get the simultaneous output of both high-precision imaging and bathymetric information, this paper proposes the multibeam synthetic aperture high-precision submarine topography imaging algorithm. It combines the imaging methods of the MBES and SAS technologies. It divides the acoustic data into groups according to the different beams to conduct aperture synthesis in each beam, and then uses the beam angle and slant range to calculate the target's depth.

As shown in Figure 5, assuming the along-track size of the real aperture is D, and the coverage width of the target area is L, this algorithm uses the combined signals received by the real aperture at different locations to synthesize a large virtual aperture.Under this condition, the transmit beam's angle of half-power point can be written as:

$$D_{\_virtual} = \frac{H_0}{\cos\beta_n}\frac{\lambda}{D} \quad \ldots (9)$$

$$\alpha_{\_virtual} = \frac{\lambda}{2D_{\_virtual}} \quad \ldots (10)$$

According to(4), (9) and (10), the along-track resolution can be written as:

$$\delta_{y\_MBSAS} = \frac{H_0}{\cos\beta_n}\alpha_{\_virtual} = \frac{D}{2} \quad \ldots (11)$$

From (11), it can be seen that the along-track resolution of the multibeam synthetic aperture high-precision submarine topography imaging algorithm is independent of the wavelength and slant distance and is only related to the size of the real aperture. The smaller the size of D, the better the along-track resolution. This algorithm uses point-by-point imaging modality to get the 3D DEM picture.

Take a single beam as an example: $\overline{p_t}$is the phase center track of the transmitting array, $\overline{p_r}$ is the phase center track of the receiving array, $\overline{p_w}$ is the scattering point coordinates, $R_t(n,\overline{p_w})$is the distance between the transmitting array and scattering point, and $R_r(n,\overline{p_w})$ is the distance between the receiving array and the scattering point. If the baseband signal is $f(t)$, the two-dimensional echo signal of the scattering point is $d_t(t,n:\overline{p_w})$after carrier wave demodulation:

$$d_t(t,n:\overline{p_w}) = \sigma_w w_t(n) w_r(n) exp\left(j\frac{2\pi}{\lambda}R(n,\overline{p_w})\right) f\left(t-\frac{R(n,\overline{p_w})}{C}\right) \quad \ldots (12)$$

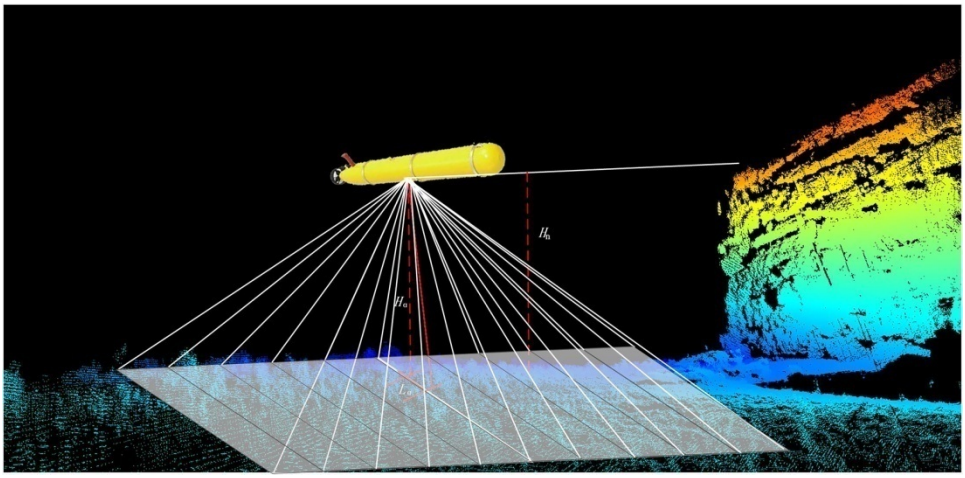

Fig. 5 — Geometric model of the multibeam synthetic aperture high-precision submarine topography imaging algorithm.

where t is the pulse duration, n is the time in the along-track direction, σ_w is the echo scattering area of the scattering point, $w_t(n)$ and $w_r(n)$ are the beam direction functions of the transmitting and receiving array, respectively, $C$is the sound speed. The slant range of the scattering point can be described as:

$$R(n,\overline{p_w}) = R_t(n,\overline{p_w}) + R_r(n,\overline{p_w}) \quad \ldots (13)$$

Hypothetically, if the transmitting and receiving arrays have good synchronization, then $w_t(n)$ and $w_r(n)$ can be replaced by $w(n)$; that is, the two-dimensional echo signal, which is compressed in the across-track direction by the matched filter. After distance compression, the two-dimensional echo signal of a single point is given by

$$d_\Pi = w(n)exp\left(j\frac{2\pi}{\lambda}R(n,\overline{p_w})\right)\chi^r\left(r - R(n,\overline{p_w})\right) \quad \ldots (14)$$

where r is the distance domain, and χ^r is the fuzzy function in the across-track direction.Additionally, after distance compression, the integral for the two-dimensional echo signal of a single point within the region of measurementsΩ is given by

$$D_\Pi(r,n) = \iiint_{\overline{p_w}\in\Omega} \sigma_w d_\Pi(r,n{:}\overline{p_w})d\overline{p_w} \quad \ldots (15)$$

After approximate discretization within Ω, (15) can be rewritten as

$$D_\Pi(r,n) \approx \sum_{\overline{p_w}\in\Omega} \sigma_w d_\Pi(r,n{:}\overline{p_w}) \quad \ldots (16)$$

Therefore, the imaging process consists of obtaining the scattering coefficient distribution in the imaging space for each scattering point by the difference of the echo signals' forms.

Results and Discussion

The experiment is carried out in an anechoic tank. The tank, with dimensionsof 25 m (L) × 15 m (W) × 10 m (H), has a six-sided silencing structure. Sound-absorbing rubber wedges are deployed all around and at the bottom of the tank. The sound-absorbing rubber wedges on the water are detachable. The rail-guided vehicle (RGV) equipment on water, which can be controlled via the electronic terminal equipment, can move thearray with three degrees of freedom (DOF) motion of the array. The RGV has two types of travel modes: Uniform motion and stop-start-stop. The minimum displacement of the RGV is 1 mm. The transmitting transducer, which has no directivity, launches an LFM signal$1ms$in width, $8kHz$ in bandwidth, and $180kHz$ in center frequency. The receiving transducer array has 80 channels. After amplification, filtering, and A/D sampling, the received data are sent to the computer for image processing.

In the experiment, the RGV works in the stop-start-stop mode with a displacement of $5mm$ at each step. A total of 160 steps in the along-rack direction are made to collect echo signals. The receiving transducer array collects 10 ping reflections and sends them to the computer for storage in each sampling position. The experimental targets are two hollow stainless-steel balls each with a diameter of $13cm$ The balls are submerged under water by heavy objects and connected with thin wire to maintain the distance between targets. The experimental layout is shown in Figure 7.

(a) (b)

Fig. 6 —(a) RGV; (b) Deployment of transducer array

The echo data are analyzed by using the multibeam synthetic aperture high-precision submarine topography imaging algorithm with the imaging area divided into 79 beams. It turns out that the two balls are located at the No. 60 beam (Fig. 8(a)) and the No. 63 beam (Fig. 8(b)).

Imaging analysis

From Figures 8 and 9, the results of MBES imaging show the balls resembling a strip, while the results of the multibeam synthetic aperture high-precision submarine topography imaging algorithm shows a better along-track resolution and the two targets can be clearly seen.

Research on sampling interval in the along-track direction

From Figures 10–13, we definitely see that different sampling intervals influence the imaging results of the multibeam synthetic aperture high-precision submarine topography imaging algorithm. The signal's main lobe has greater influence in the along-track direction after processing with a larger sampling interval. The main lobe widens in the along-track direction at the expense of the peak amplitude's decline. From the viewpoint of energy, the broadening of the main lobe means an increase of energy. However, it is not sufficient to compensate for the energy loss caused by the decline of the main lobe's peak amplitude. Therefore, the total energy of the main lobe decreases. The amplitude of the grating lobe increases after processing with a larger sampling interval, such that the total energy of the grating lobe increases. Essentially, energy mostly remains constant while transmitting from the main lobe to the grating lobe because of the under-sampling in the along-track direction.

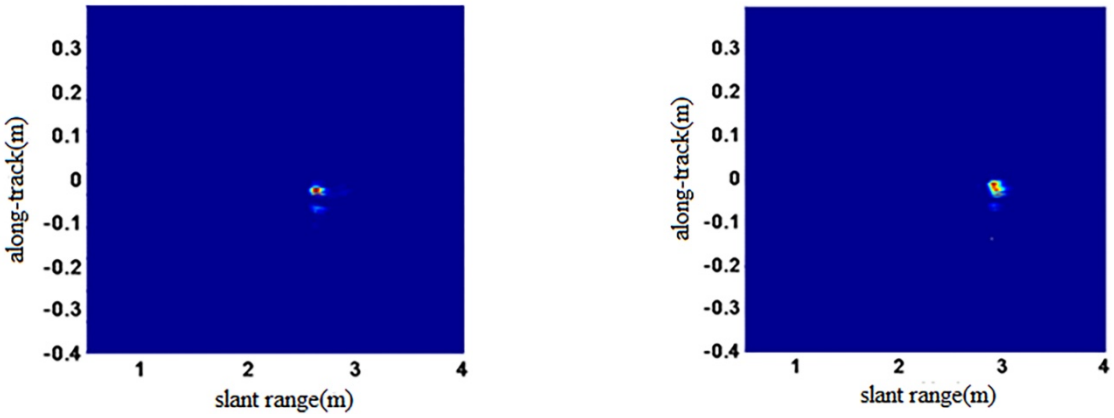

(a) (b)

Fig. 8 —The multibeam synthetic aperture high-precision submarine topography imaging algorithm imaging of the No. 60 beam (a) and the No. 63 beam (b).

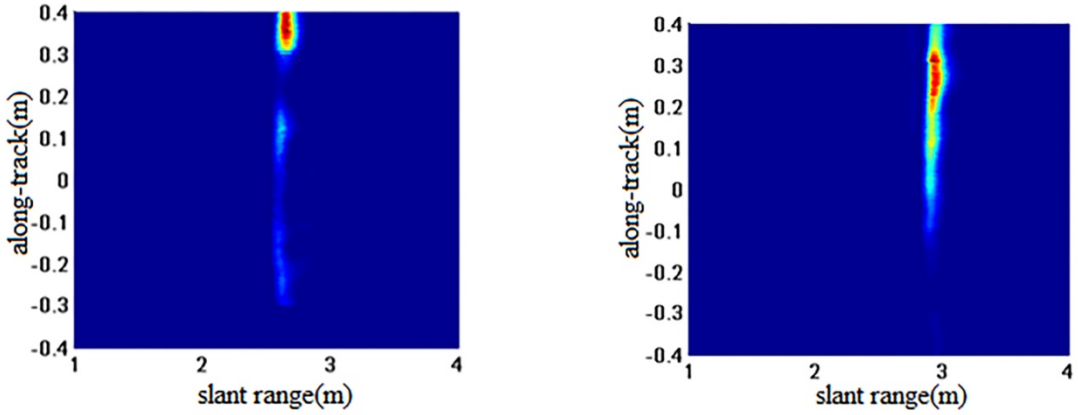

(a) (b)

Fig. 9 —The MBES imaging of the No. 60 beam (a) and the No. 63 beam (b).

Further validation

To further verify the effectiveness of the algorithm, we also conducted experiments under the same conditions with the exception that the two targets are both deployed in the along-track direction. As shown in Figure 14, the multibeam synthetic aperture high-precision submarine topography imaging algorithm and the SAS can both distinguish the two targets in the imaging results, while the energy distribution of the multibeam synthetic aperture high-precision submarine topography imaging algorithm is more concentrated. The imaging result of the MBES is not

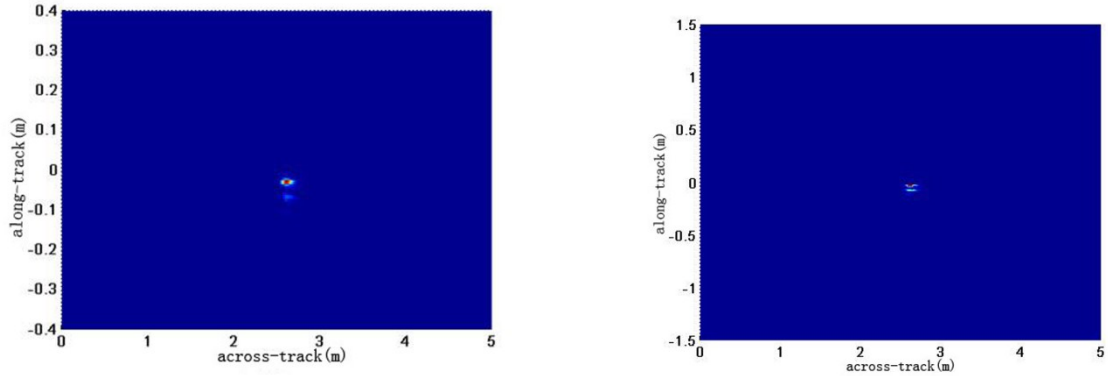

(a) Partial (b) Overall

Fig. 10 — Imaging results of the multibeam synthetic aperture high-precision submarine topography imaging algorithm (regular sampling interval)

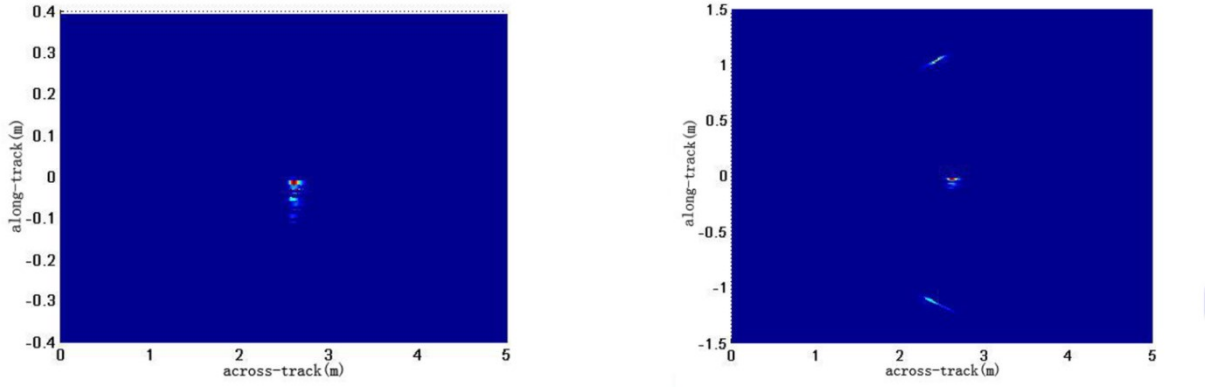

(a) Partial (b) Overall

Fig. 11 —Imaging results of the multibeam synthetic aperture high-precision submarine topography imaging algorithm (double sampling interval)

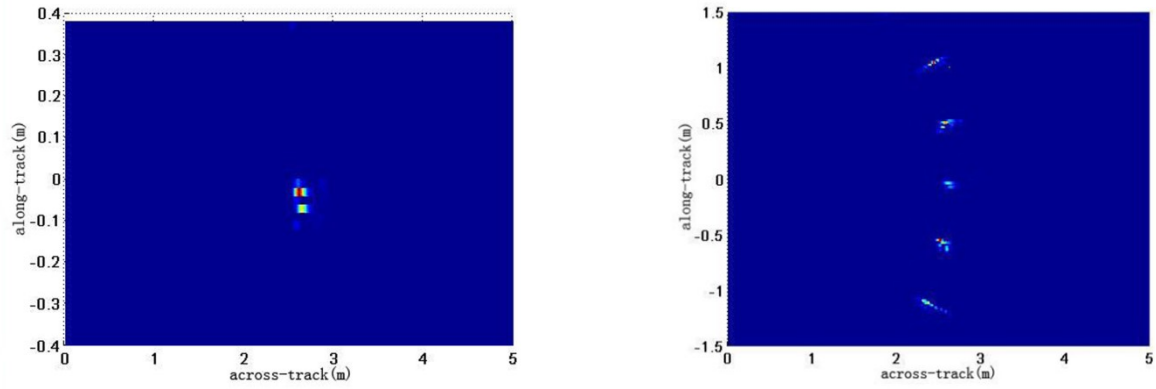

(a) Partial (b) Overall

Fig. 12 —Imaging results of the multibeam synthetic aperture high-precision submarine topography imaging algorithm (four times the sampling interval)

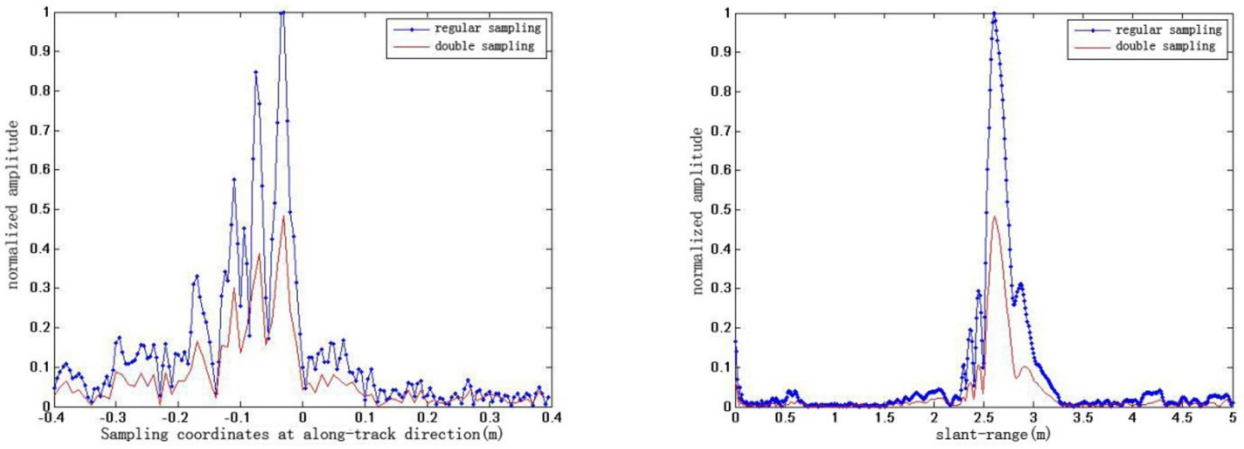

(a) Along-track (b) Across-track

Fig. 13 —Comparison between processing results of the multibeam synthetic aperture high-precision submarine topography imaging algorithm with different sampling intervals

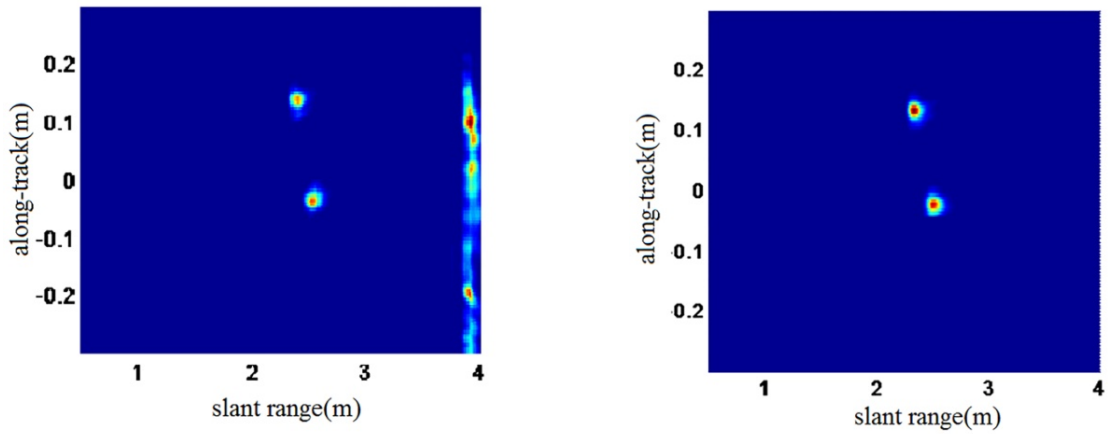

(a) (b)

Fig. 14 —(a) SAS imaging results; (b) The multibeam synthetic aperture high-precision submarine topography imaging algorithm imaging results.

shown because of the poor resolution of the along-track direction, as discussed before.

Conclusion

This paper presented research on a new algorithm for high-precision submarine topography imaging, its tank experiment and imaging results. The following conclusions can be made:

- The multibeam synthetic aperture high-precision submarine topography imaging algorithm retains the synthetic aperture's high resolution in the along-track direction, and it can obtain the target's bathymetric information after beamforming.
- The energy distribution of the multibeam synthetic aperture high-precision submarine topography imaging algorithm is more concentrated than the SAS method. It has an inhibitory effect on the clutter signal outside of the beam in which the target exists.
- The multibeam synthetic aperture high-precision submarine topography imaging algorithm is also restricted by the sampling interval in the along-track direction in practical application. When the sampling interval used in the processing is larger than the regular sampling interval, the impact is mainly manifested in the along-track direction. The main lobe widens in the along-track direction with the decline of the peak amplitude. Part of the energy is transmitted to the grating lobe.

Based on the confirmation of the accuracy of the imaging results, the advantages of the multibeam synthetic aperture high-precision submarine topography imaging algorithm are reflected by the comparative analysis.

Acknowledgement

This study was supported by the National Natural Science Foundation of China (41706106, 41376103).

References

1 Qihu, Li . "Advances of research work in some areas of underwater acoustics signal processing." *Applied Acoustics* (2001).

2 Ura, Tamaki . "Observation of Deep Seafloor by Autonomous Underwater Vehicle." *Indian Journal of Geo Marineences* 42.8(2013) 1028-1033.

3 Pailhas, Yan , Y. Petillot , and B. Mulgrew . "Increasing circular synthetic aperture sonar resolution via adapted wave atoms deconvolution." *The Journal of the Acoustical Society of America* 141.4(2017) 2623-2632.

4 Ge, Yu , and P. Shengchun . "Multiple Moving Targets Detection and Parameters Estimation in Strong Reverberation Environments." *Shock and Vibration* 2016(2016) 1-10.

5 Shahrestani, Suzan , et al. "Detecting a nearshore fish parade using the adaptive resolution imaging sonar (ARIS): An automated procedure for data analysis." *Fisheries Research* 191(2017) 190-199.

6 Bulmer, M. H , and J. B. Wilson . "Comparison of flat-topped stellate seamounts on Earth's seafloor with stellate domes on Venus using side-scan sonar and Magellan synthetic aperture radar." *Earth & Planetary Science Letters* 171.2(1999) 277-287.

7 Lee, Hua . "Motion compensation by phase correction for synthetic-aperture side-scan sonar imaging." *International Journal of Imaging Systems & Technology* 14.6(2004) 259-261.

8 Asada, A. . "Expanded interferometry and synthetic aperture applied to a side scanning sonar for seafloor bathymetry mapping." *Proc. of 2004 International symposium on Underwater Technology UT04 IEEE*, 2004.

9 Li, Haisen , et al. "Underwater acoustic / optical imaging system." *IEEE International Conference on Signal Processing*, 2010.

10 Sun, Wei , et al. "Study of multibeam synthetic aperture interferometric imaging algorithm." *International Industrial Informatics & Computer Engineering Conference* 2015.

11 Liu, W. , C. H. Zhang , and J. Y. Liu . "Research on synthetic aperture sonar 3-D data simulation." *Journal of System Simulation* 20.14(2008) 3838-3841.

12 Sharaga, Nathan , J. Tabrikian , and H. Messer . "Optimal Cognitive Beamforming for Target Tracking in MIMO Radar/Sonar." *IEEE Journal of Selected Topics in Signal Processing* 9.8(2015) 1440-1450.

13 Thode, Aaron M. , et al. "Acoustic vector sensor beamforming reduces masking from underwater industrial noise during passive monitoring." *The Journal of the Acoustical Society of America* 139.4(2016) EL105-EL111.

14 Xiao, Liu , et al. "Multibeam seafloor imaging technology based on the multiple sub-array detection method." *Journal of Harbin Engineering University* (2012).

15 Zhou, T. , et al. "Research on the multiple subarray-pairs interferometric algorithm used in high resolution multibeam bathymetric system." *Journal on Communications* (2010).

16 Williams E. *Fourier Acoustics*,(Academic Press) 1999.

17 Jackson, Darrell R., et al. *High-Frequency Seafloor Acoustics*,(Springer, New York, NY) 2007.

18 Kargl, S. G. , K. L. Williams , and E. I. Thorsos . "Synthetic Aperture Sonar Imaging of Simple Finite Targets." *IEEE Journal of Oceanic Engineering* 37.3(2012) 516---532.

19 Bird, J. S. , and G. K. Mullins . "Bathymetric Sidescan Sonar Bottom Estimation Accuracy: Tilt Angles and Waveforms." *IEEE Journal of Oceanic Engineering* 33.3(2008) 302-320.

20 De Moustier, C. "Empirical uncertainty in angle of arrival estimation for bathymetric sidescan sonars." *Oceans 2011*.

21 Kraeutner, P H , et al. "Multiangle Swath Bathymetry Sidescan quantitative performance analysis." *Oceans IEEE*, 2002.

22 Xu, Wen , and W. K. Stewart . "Coherent source direction estimation for three-row bathymetric sidescan sonars." *Oceans IEEE*, 1999.